

## Compaction bands simulated in Discrete Element Models

G. Marketos\*, M.D. Bolton

*Geotechnical and Environmental Research Group, Engineering Department, University of Cambridge, UK*

### ARTICLE INFO

#### Article history:

Received 16 June 2008

Received in revised form

12 February 2009

Accepted 2 March 2009

Available online 12 March 2009

#### Keywords:

Compaction bands

Discrete Element simulations

Grain breakage and crushing

Localisation

Sandstone

### ABSTRACT

Compaction bands, i.e. tabular zones that accommodate compaction but no shear, have recently been observed in high-porosity sandstone, where the dominant micromechanism is grain breakage and crushing. Such bands are extremely important for hydrocarbon extraction, forming barriers that might inhibit the flow. They have further been associated with borehole stability problems. However, compaction band initiation and propagation remain poorly understood, while the necessary material conditions for their formation require further investigation.

Three-dimensional Discrete Element Method simulations of the stressing of a sandstone sample were conducted. These successfully reproduced a discrete compaction band; its initiation and propagation are shown. An investigation into the effects of the cementation bond strength and the post-fragmentation behaviour of the grains on the observed behaviour is also presented. Well-localised discrete bands were observed when both the bond strengths were high and the grains lost their load-bearing capacity after being broken. On the contrary, an advancing crushing front resembling a diffuse compaction band was observed in simulations where the broken grain could still carry force. The data presented here provide the micromechanical insight necessary for a better understanding of conditions leading to compaction band initiation and propagation, which might facilitate identification of rocks that might form them.

© 2009 Elsevier Ltd. All rights reserved.

### 1. Introduction

Compaction bands are thin tabular zones that display localisation of compressive strain accompanied by no shear offset of the top relative to the bottom layer. They have only recently been identified in porous sandstone (Mollema and Antonellini, 1996) and have been associated with unstable material behaviour, as band formation is accompanied by stress-drops in strain-controlled laboratory tests (e.g. Baud et al., 2004). Compaction bands can also occur in a variety of other materials (see Holcomb et al., 2007, for a summary). Nevertheless, the current study will focus on compaction bands forming in high-porosity quartz sandstone, where the dominant micromechanical phenomenon is grain breakage and crushing.

Compaction bands have an immense practical importance, as they form in materials often encountered in hydrocarbon reservoirs. They are associated with a large porosity reduction, and so can reduce the gross permeability of the parent material by at least two orders of magnitude (e.g. Vajdova et al., 2004). At the reservoir scale this might lead to increase in the required pressure gradient

by up to three times so as to maintain a required flow rate at the well (Sternlof et al., 2006). One can further imagine that compaction bands might compartmentalise the reservoir, trapping the hydrocarbons. This is significant as compaction bands can form during pore-fluid extraction. Haimson (2001) further linked compaction bands to borehole break-outs. He observed that fluid flow into the well could remove the grain fragments produced in the band, thus implying a link between compaction bands and sand production at the oil-well.

However, little is known about the grain-scale properties and rock microstructural attributes necessary for compaction band formation, or about the way that these features initiate and propagate. Consequently little can be said about whether a specific sandstone will form compaction bands or not, and at what stress level.

### 2. A summary of insight from available data and questions unanswered

Compaction bands in sandstone have in all cases been associated with extensive grain crushing and microcracking. Thus there is a limiting mean effective stress below which compaction band formation is impossible. The observation of pure compaction localisation (i.e. no shear) also depends on the exact stress (or strain) path the material is subjected to. It is generally accepted that they form only in high-porosity sandstone.

\* Corresponding author. Present address: Geology and Geophysics Group, National Oceanography Centre, European Way, Southampton SO14 3ZH, UK. Tel.: +44 2380596614.

E-mail address: [g.marketos@noc.soton.ac.uk](mailto:g.marketos@noc.soton.ac.uk) (G. Marketos).

Recent research on compaction bands has raised a number of important questions. For example, the grain damage observed in the laboratory is more severe than what has been observed in the field. In addition, there seem to be some differences between the rapid and unstable band propagation in experiments, and its inferred propagation from field data (see Mollema and Antonellini, 1996 and Sternlof et al., 2005).

Another important question is whether compaction bands would form in unbonded, sandy sediments. Sternlof et al. (2005) used geological evidence to hypothesise that negligible cementation existed between the grains during compaction banding, implying the possibility of compaction band formation in sands. No compaction bands have been identified so far in experiments on sand. However, it is highly probable that the unstable behaviour observed by Hyde and Nakata (1999) during a one-dimensional compression test on a collection of uniformly sized glass beads could be due to localised grain crushing.

Further confusion arises from features sometimes termed *diffuse compaction bands* (e.g. Olsson and Holcomb, 2000 and DiGiovanni et al., 2001). These are essentially localised compaction fronts that were observed in the laboratory. They initiated at the sample boundaries (probably due to a lower grain density leading to larger inter-grain contact forces) and propagated through the sample in the principal straining direction. As diffuse compaction bands have not been documented in the field it is unclear whether such behaviour is an artefact of the experimental technique. Furthermore, the reasons why some sandstones form discrete while others form diffuse bands are still unknown.

Olsson et al. (2002) hypothesised that the different orientation of the major stress relative to the bedding direction was to blame. On the other hand, Katsman and Aharonov (2006) suggested that a wide distribution of grain crushing strengths might be responsible for the diffuse crushing localisation. Baud et al. (2004) further suggested that diffuse compaction bands might well be a large number of smaller sequentially produced discrete bands whose propagation was somehow blocked by the sandstone microstructure. It is unknown which, if any, of these hypotheses are correct; in the light of data from new simulations, an additional micro-mechanical explanation will be proposed in Section 4.1 below.

As discussed above, the material properties essential for a sandstone to form compaction bands are still unknown. Various continuum mechanics methods (e.g. Issen, 2002) were developed to this aim, and have concluded that only materials with a cap in the yield surface can form compaction bands. Further, Rudnicki and Sternlof (2005) have treated a propagating band as a closing crack and more recently Rudnicki (2007) has used an anti-crack/anti-dislocation model, which has been successful in predicting the relation between band length and band thickness (see Tembe et al., 2008). These methods have linked material behaviour to the constitutive model parameters, or other continuum mechanics quantities. As the link between the above and the grain physical properties remains elusive, in order to be able to predict whether and when a sandstone would form compaction bands an extensive laboratory testing program would need to be implemented so as to establish the shape of its yield surface, or the exact value of these continuum mechanics quantities.

The most promising approach to linking grain properties to the observed macroscopic behaviour seems to be the direct micro-mechanical modelling of compaction band formation. A step in this direction was taken by Katsman and Aharonov (2006), who conducted simulations on a two-dimensional analogue of a porous material made up of a regular network of linear springs. However, even though invaluable insight was gained, this model again did not model each grain separately but linked the behaviour to equivalent properties for assemblies of 5–10 grains.

This article will present results of three-dimensional Discrete Element Method (DEM) simulations of the stressing of granular samples which reproduced breakage localisation and compaction bands. The sole inputs to such simulations are the grain physical properties, and as each grain is modelled separately, the complete micromechanism of deformation can be reproduced in a well-controlled, repeatable environment. DEM also allows for the examination of the initiation and propagation of a band with detail that would be impossible in the laboratory.

In addition, the DEM code allows easy access to the multitude of data involved, yielding information on micromechanical parameters of interest (such as the internal grain-force distribution) which would otherwise be inaccessible. Furthermore, parametric studies can easily be performed with precisely the same initial conditions, allowing for the identification of the effect of any grain-scale quantity on the observed behaviour. The potential of the DEM method has been demonstrated by Wang et al. (2008) who report the results of two-dimensional Discrete Element Method (DEM) simulations of compaction bands in a bonded granular material. For example, Wang et al. observed the micromechanism of damage localisation in their rock model and confirmed that increased grain uniformity increased the probability of discrete compaction band formation.

The novelty of the work presented here is that as the DEM simulations were three-dimensional the full micromechanism of grain breakage localisation was observed. In addition two further parametric studies will be presented here, one to investigate the effect of grain cementation on compaction band formation, and the other to investigate the effect of the fragmentation mode of each grain, neither of which had previously been considered. These will be shown to provide possible answers to the two important questions set out above, namely, whether compaction banding is possible in sands, and why diffuse compaction bands are formed.

### 3. The Discrete Element Method (DEM)

The commercially available PFC<sup>3D</sup> software package was used for the three-dimensional Discrete (or Distinct) Element Method (DEM) simulations presented here. The main modification to the available code was the implementation of a grain breakage and crushing model. PFC<sup>3D</sup> is based on the initial work of Cundall and Strack (1979) and is described in more detail in the PFC<sup>3D</sup> manual (Itasca Consulting Group Inc., 2003). It is important that the DEM parameters be of the correct order of magnitude. Their selection is discussed in Marketos (2007), and their values are shown in Table 1.

#### 3.1. The granular sample

The sample used in the simulations (see Fig. 1a) consisted of 8943 spherical particles whose radii were uniformly distributed between 1 and 2 mm. Grains interacted with each other at their

**Table 1**  
Micromechanical parameters used for the simulation.

Parameter	Numerical value
Normal and shear stiffness of balls	$4 \times 10^6$ N/m
Normal and shear stiffness of walls	$4 \times 10^6$ N/m
Particle friction coefficient, $\mu_b$	0.5
Wall friction coefficient, $\mu_w$	0.0
Density of spheres	2650 kg/m <sup>3</sup>
Coefficient of local damping	0.7
Sample shortening rate (uniaxial)	100 mm/s
Grain strength	40 MPa
Bond stiffness per unit area, $\kappa$	$5 \times 10^{12}$ N/m <sup>3</sup>
Ratio of bond radius to grain radius	0.4

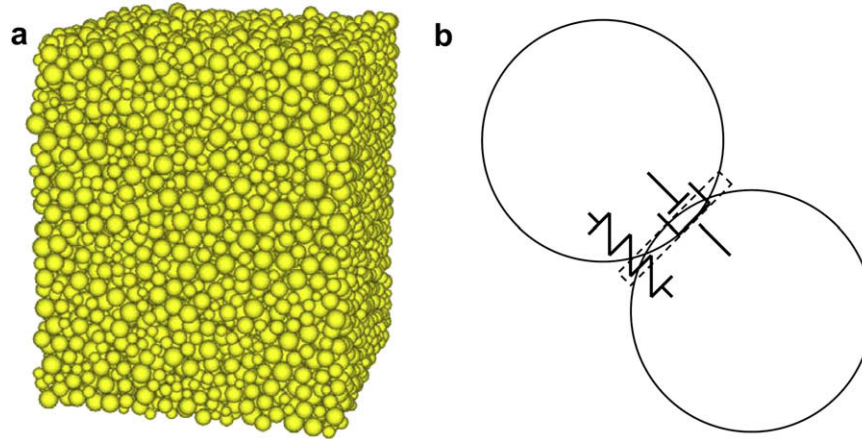


Fig. 1. (a) The granular sample used in the simulations presented here in its unstressed state. (b) A sketch of a 2-grain model in DEM.

mutual contact (see Fig. 1b). The sample had initial dimensions of  $60 \times 60 \times 72$  mm and an initial porosity of 45.7%, when completely unstressed. This corresponds to a voids ratio of 0.84. It was bounded by frictionless flat walls of the same normal stiffness as the sand grains ( $4 \times 10^6$  N/m).

The sample was generated by numerically simulating the ‘dry pluviation’ experimental sample preparation technique. This preparation method resulted in a loose sample and is thought to replicate well the slow sedimentation of grains under gravity. The resulting granular structure was analysed by inspecting the angle  $\phi$  between the vertical (positive  $z$  axis) and the contact normal direction, and the angle  $\theta$  between the positive  $x$  axis and the projection of the contact normal direction on the  $x$ - $y$  plane. In calculating  $\phi$  and  $\theta$ , contacts with the sample walls were neglected and the contact direction was taken always to point upwards, so as to avoid ambiguity. The latter meant that  $\phi$  could vary from  $0^\circ$  to  $90^\circ$ , and  $\theta$  from  $-180^\circ$  to  $180^\circ$ . The granular fabric was found to be anisotropic (transversely isotropic) as can be seen in Fig. 2, produced for the sample at its unstressed state.

3.2. The crushing model

There is no standard way of modelling grain breakage and crushing in DEM simulations, and so a number of schemes have been proposed (e.g. Cheng et al., 2003; Couroyer et al., 2000; Tsoungui et al., 1999). All such schemes rely on some simplifying assumptions in order to capture the behaviour without dramatically increasing computation time. In the scheme used here the

simulation was started with a number of spheres equal to the number of grains initially in the sample. A criterion was pre-selected that dictated when a particle would fragment, depending on the stress levels inside it.

3.2.1. The breakage criterion

The breakage criterion in DEM is frequently defined in terms of the contact forces acting on the grain (Couroyer et al., 2000; Tsoungui et al., 1999; Lobo-Guerrero and Vallejo, 2005) as in most cases a specific value of stress inside the grain will initiate failure at a grain flaw. The variability in both the size and location of the flaw in similar grains can then be described by the assignment of a specific distribution to a single stress-like parameter, the strength of the grain. The strength of grains has been experimentally investigated by a number of researchers who conducted sets of single-grain crushing tests (e.g. McDowell and Amon, 2000; Nakata et al., 1999, 2001; Takei et al., 2001).

In the simulations here a grain was set to break if the characteristic stress inside it (defined as the ratio of the maximum normal contact force on the particle and the square of its diameter) exceeded its crushing strength value (see Eq. (1)). A very similar grain breakage criterion was used by Couroyer et al. (2000) in three-dimensional DEM simulations.

$$\sigma_{\text{crush}} \geq \sigma_{\text{ch}} = \frac{F_{\text{max particle}}}{D^2}, \text{ grain breaks otherwise} \quad (1)$$

The above breakage criterion relates the tensile stress inside a grain to a single scalar descriptor of the contact force set it is

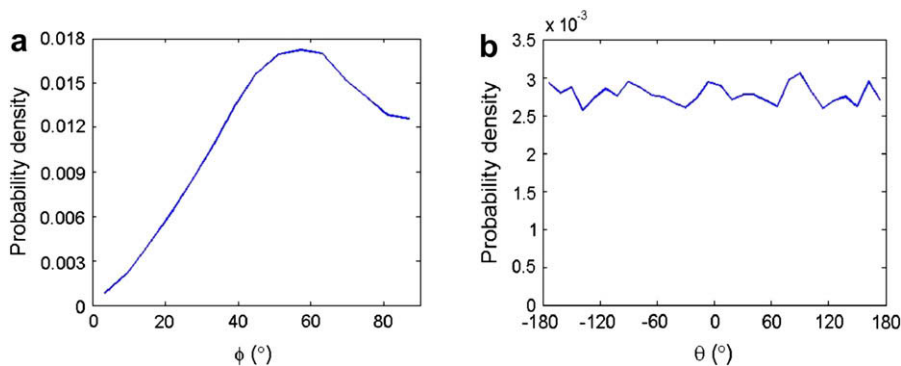


Fig. 2. The probability density plots for the angle between (a) the inter-particle contact normal and the vertical,  $\phi$ , and (b) the projection of the inter-particle contact normal on the  $x$ - $y$  plane and the positive  $x$  axis,  $\theta$  for the sample.

subjected to. The effect of the spatial distribution of the contact forces around the grain is thus neglected. However, this effect is thought to be irrelevant to the current study where the granular structure is rather loose and the coordination number of approximately two-thirds of the grains is either 4, 5 or 6.

### 3.2.2. Post-breakage behaviour

In the simulations reported here three different methods were used to model the fragmentation of a grain, each of which implies a different grain fragmentation mode. In some of the simulations presented here the crushing of the particles was modelled simply by removing them, following Couroyer et al. (2000). Particle removal is thought to represent cases where the parent grain crushes into dust that falls into the large inter-particle void space. The dust would then have a negligible effect on the behaviour of the granular sample immediately after the crushing event; large strains would be required in order for the fragments to carry stress once more. Such a method would not reproduce the stiffening of the sample at large strains, but is sufficient for the study of compaction band formation, which occurs over a relatively small strain interval.

The second method involved introducing fragments into the granular sample, so as to replace the broken grain. A similar scheme was employed in two-dimensional simulations by Tsoungui et al. (1999) and Lobo-Guerrero and Vallejo (2005). Here, the arrangement shown in Fig. 3 was used as a compromise between number of fragments (8) and the percentage of the original volume (47.2%) that these filled was sought. After each breakage event the broken grain was removed and 8 particles were introduced in its place, centred at its centroid and arranged in the configuration of Fig. 3. The fragments' radii were scaled so as to ensure that the 8-grain assembly would fit inside the sphere representing the initial particle. Particle replacement was equivalent to approximately half the mass of a broken grain turning into dust, but meant that the grain fragments could now carry force. A random rotation was applied to the configuration of Fig. 3 to simulate the random orientation of the internal flaws leading to breakage. A radius limit was also implemented (here 0.25 mm), below which particles could no longer fragment. This represents a comminution limit,

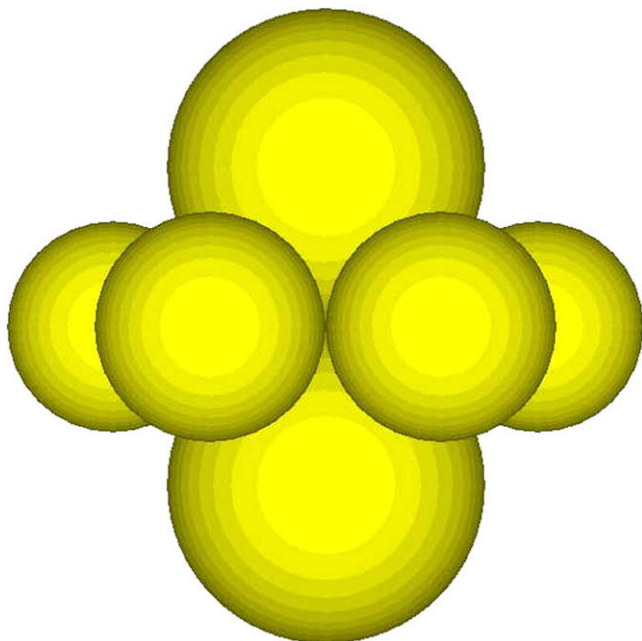


Fig. 3. The fragment configuration consisting of 8 fragments of two different sizes.

a size below which the grains become so strong, due to the absence of internal flaws that they no longer fracture.

In reality, the number of fragments of a grain will be highly variable, depending on the mineralogy and presence of internal flaws inside grains. Takei et al. (2001) reported that glass beads were found to shatter between 30 and 50 pieces, further confirming that particle removal can suitably model their fragmentation behaviour. However, for sand quartz particles Takei et al. reported a highly variable but smaller number of fragments per particle (less than 10 in most cases). As the fragment size distribution is not always very realistic, the simulations will fail to capture the grain size evolution of the sample. Nevertheless, by introducing the grain fragments, the local post-breakage stiffening after a grain breakage event can be modelled.

The third method for modelling grain breakage involved reducing the contact stiffness of a grain by some factor (here this was arbitrarily set to 2), while grains were only allowed to break once. The stiffness reduction value depends on grain mineralogy and the lateral confinement provided to the fragments by neighbouring particles. Grain stiffness reduction was implemented to simulate cases where the fragments could still carry some force immediately after breakage, with deformation of inter-fragment voids making the local response less stiff. Additionally all parallel bonds at the contacts of the broken particle were deleted, causing a further, small contact stiffness reduction. This method had the added advantage of reducing the local implosive behaviour observed on particle removal for both the previous grain breakage methods. One should note that no single breakage model is more correct than the others; they each relate to different classes of real grain behaviour which might be caused by different grain mineralogies or intra-grain crystal structures.

### 3.3. Strain application and sample boundaries

The DEM sample was tested under one-dimensional (uniaxial) compression in the absence of gravity, with a vertical shortening rate of 100 mm/s, giving a compressive strain rate of  $1.39 \text{ s}^{-1}$ . The use of a large strain rate was dictated by the need to minimise computation time, but was seen by Marketos (2007) not to affect DEM results qualitatively but only to introduce small quantitative changes in other simulations, affecting just the initial stressing of the granular sample.

An issue in DEM simulations and in laboratory tests on granular materials is the question of boundary effects. Here the use of a flat boundary for stressing the sample will lead to a locally smaller solid density adjacent to it, as the flat boundary disrupts the granular packing (see Hardin, 1989 and Marketos and Bolton, submitted for publication). This is even more significant when grain breakage is expected, since breakage will preferentially occur close to the flat boundaries (see e.g. Marketos and Bolton, 2005) with the locally looser structure resulting in a larger force per grain. In order to suppress this grain damage localisation, grains in a region extending 3 mean diameters (9 mm) from the top and bottom flat boundaries were not allowed to fragment. In addition, the grains were left unbonded in the 9 mm wide boundary region. This allowed for a more random stress transmission from the boundary to the bulk of the sandstone.

## 4. Simulations of grain crushing and bond cracking in sandstone

A set of simulations was performed on the sample with particles cemented together by parallel bonds so as to model a sandstone rock. One should recall that in PFC<sup>3D</sup> the parallel bond adds to the contact stiffness, and can break both in tension, compression or

shear when the stress inside it exceeds its strength. A total of 19,742 bonds (i.e. 2.9 bonds per grain) were installed in the sample. Bonds were installed at contacts between particles when the sample was in its unstressed state.

The simulated sandstone had a  $K_0$  value (the ratio of radial to axial stress in one-dimensional compression) of 0.15, corresponding to a Poisson ratio of 0.13 assuming an isotropic elastic material. The first simulation was performed with a uniform characteristic particle crushing strength of 40 MPa, accompanied with particle removal after crushing. The bond strength was chosen initially as large (400 MPa) in order to investigate the effect of relatively unbreakable bonds on the observed behaviour.

The stress–strain curve for this simulated sandstone is shown in Fig. 4a. The bond cracking and grain crushing rate are also shown. Here one can observe a large stress-drop, associated with a surge in crushing events. Negligible cementation bond breakage occurred before the stress-drop, indicating that the initial material structure remained intact. The locations of crushing events during this stress-drop are plotted in Fig. 4b. One can observe that the 357 crushes that occurred during decreasing macroscopic stress formed a band perpendicular to the straining direction. This feature was undoubtedly a compaction band, as a whole layer of stress-bearing particles was crushed.

4.1. The influence of fragments

Two additional simulations were performed, with precisely the same initial conditions and loading rate, the only difference being the post-breakage behaviour of a particle. Previously the particles were removed in order to model their reduction to a set of dust-sized pieces. In the first additional simulation the parent particle was replaced by 8 smaller spheres of two different sizes after breakage (see Fig. 3 and Section 3.2.2). In the second additional simulation particle breakage was modelled by a reduction of the particle contact stiffness by a factor of 2, while particles already broken were not allowed to break more. Also, all parallel bonds at the contacts of the broken particle were deleted, providing for a further, small contact stiffness reduction.

The stress–strain curves for the simulations with a modified post-breakage grain behaviour are compared in Fig. 5. Here one observes that the modelling of the grain fragments had a very small effect on the observed behaviour. The sample became unstable at exactly the same point, and the stress-drop continued to be large but was slightly reduced (by 7%). Furthermore, the compaction band was confirmed to form at the same location. This points to the fact that, as the fragments fell into the pore space, they were unable

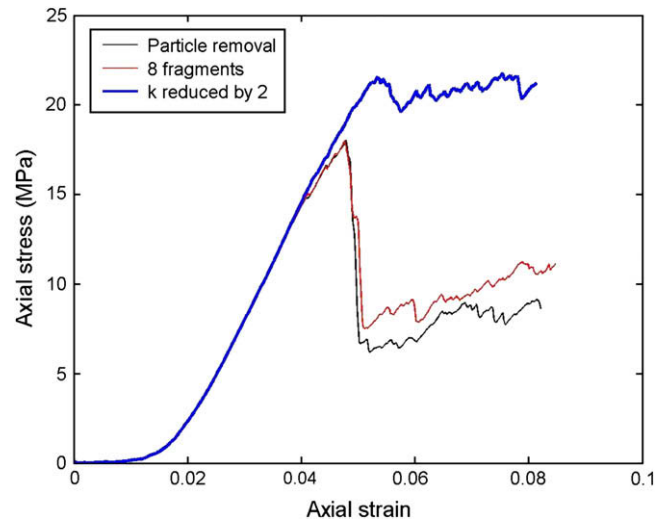


Fig. 5. The stress versus strain for the simulations performed with a modified post-breakage grain behaviour and a large cementation bond strength (400 MPa).

to carry force in the small strain increments associated with compaction band formation.

However, the fragments had an effect on the post-band behaviour. In the simulations including particle replacement, the crushing locations after sample instability were seen to remain concentrated in the location of the original band. Now it was the fragments that crushed, as seen in Fig. 6. This indicates that the compaction band first formed and then accommodated additional crushing. This seems to agree with field observations, which link an increased degree of grain breakage to an increased maturity of the compaction band (which in the field manifests itself as an increase in band length). One should note, however, that the choice of the grain breakage criterion might affect post-localisation behaviour, something that was not studied here.

Fig. 5 also suggests that modelling grain breakage by reducing the contact stiffness by a factor of 2 had a stabilising effect, as the large stress-drop associated with compaction band formation could no longer be observed. Smaller stress-drops were observed nevertheless, and it was separately confirmed that these corresponded to fairly localised crushing. However, overall, the features of this crushing localisation were found to be very different to the ones previously encountered.

Fig. 7 plots the height above the bottom boundary for each crushing event against the strain at which it occurred. The

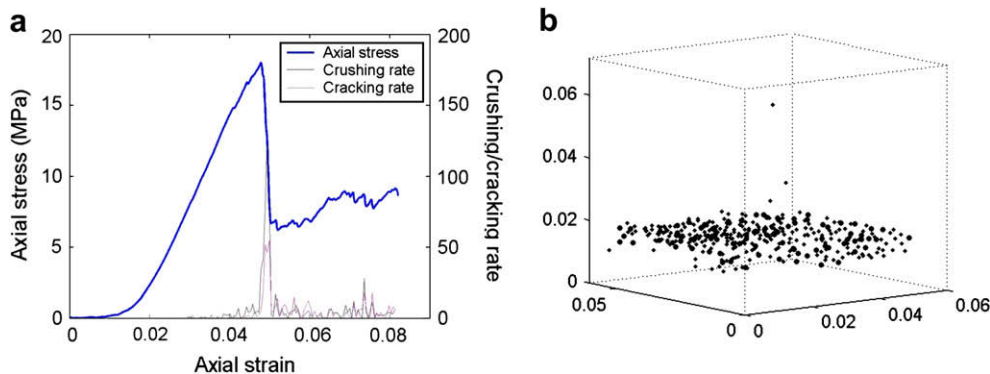


Fig. 4. (a) The stress, crushing and cracking rate versus strain for the sandstone simulation with a bond strength of 400 MPa, and where crushing is modelled by particle removal. (b) A plot of the crushing locations during the stress-drop observed in (a). Sample dimensions in meters.

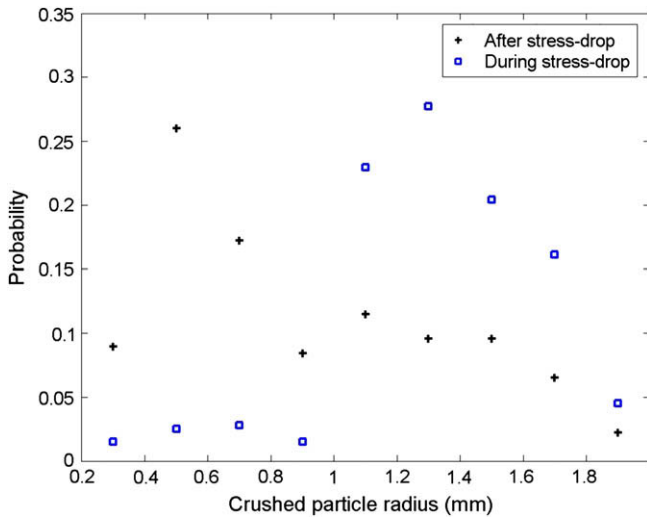


Fig. 6. The probability distribution of the crushed particle radius during and after the stress-drop for the simulation where the particle fragments were introduced (a comminution limit of 0.25 mm was implemented).

$z$ -coordinate was plotted as it is the only relevant coordinate. This is because any crushing localisation features should be compatible with the externally applied displacement field, i.e. should be parallel to the  $x$ - $y$  plane. In this figure one observes that crushing initiated at the top and bottom boundaries. However, after a strain of 0.05, crushing events seemed to be clustered with the cluster centroid moving upwards as strain increased.

This was confirmed by the plot of the mean height of all crushes in a specific strain interval versus strain (see Fig. 7). Here one observes that after a strain of 0.05 the centroid moved with a roughly constant velocity through the sample. Therefore one might deduce that the situation here was very similar to the observation of a crushing front advancing through the sample in diffuse compaction bands of the type reported by Olsson and Holcomb (2000) and DiGiovanni et al. (2001). However, the crushing front was not so pronounced as in the laboratory tests.

Even so, Fig. 7 allows for an estimate of the velocity of the crushing centroid. The gradient ( $\Delta z/\Delta \epsilon$ ) of a line fitted to the data

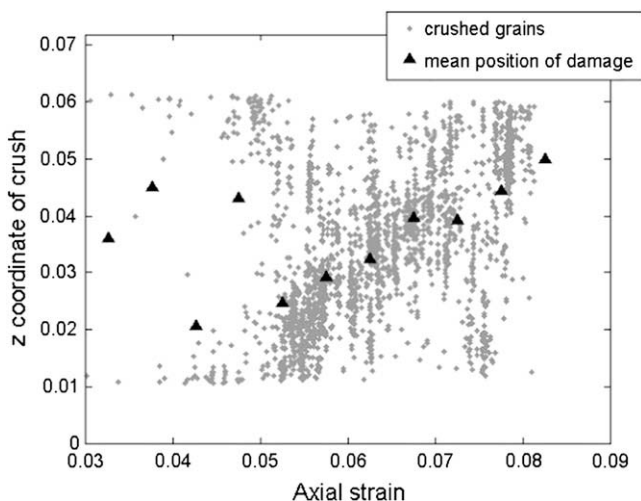


Fig. 7. The height of each crushing event plotted against the strain at which it occurred for the simulation where crushing was modelled by halving the grain-contact stiffness.

for strains larger than 0.05 is approximately 0.8 m. This gradient can be related to the velocity of the front ( $\Delta z/\Delta t$ ) by Eq. (2).

$$\frac{\Delta z}{\Delta t} = \frac{\Delta z}{\Delta \epsilon} v = 0.8 \text{ m} \frac{0.1 \text{ m/s}}{0.07 \text{ m}} = 1.2 \text{ m/s} \quad (2)$$

where  $v$  is the velocity of the top platen relative to the bottom and  $l$  is the initial height of the sample. Using Eq. (2) the crushing front velocity can be calculated as 1.2 m/s, 12 times larger than the sample shortening rate. Olsson (2001) reports the observation of a crushing front velocity 8 times larger than the sample's shortening rate. Olsson further links the ratio of the crushing front velocity as divided by the platen velocity to the porosity reduction behind the crushing front through Eq. (3) below, in which  $\phi$  denotes porosity and  $u$  velocity.

$$\frac{u_{\text{front}}}{u_{\text{platen}}} = \frac{1 - \phi_{\text{after}}}{\phi_{\text{before}} - \phi_{\text{after}}} = \frac{1 - 0.408}{0.433 - 0.408} = 24 \quad (3)$$

Substituting into Eq. (3) the porosity values calculated from our simulations at strains close to the initiation of the crushing front ( $\epsilon_{zz} = 0.048$ ) and close to the end of its propagation through the sample ( $\epsilon_{zz} = 0.081$ ) we obtain a prediction of the velocity ratio using this model. This is of the correct order of magnitude but double the value observed in the simulations, indicating that Olsson's simplified model is not directly applicable to the case presented here. The complications arise from the fact that in our simulations the sandstone is made up of grains of variable strength, with only the weaker grains suffering damage as the crushing front moves through the sample. Remembering that for this breakage criterion once a grain breaks it cannot break further, grain damage propagates inwards as weak grains at a specific vertical level get depleted. Therefore, further to porosity change and platen speed, the speed of the crushing front must also depend on the spatial distribution and relative probability of existence of the weaker grains. This has not been incorporated in Olsson's (2001) model, hence the discrepancy.

The simulation results shown in this section highlight the importance of the grain fragments' stiffness and the fragmentation mode on the crushing localisation evolution. It seems here that whenever the grain fragments cannot carry stress immediately after breakage the material becomes locally unstable, resulting in a macroscopic stress-drop and a well-defined discrete compaction band. This can also happen when the fragment size is much smaller than the pore-size, as in the case of the simulations where the parent particle was replaced by 8 smaller ones. This is in contrast with the case where breakage was simulated by a contact stiffness reduction of 2, where the sample behaviour was much more stable and the crushing localisation much less marked, resembling diffuse compaction bands as observed in experiments. However, the formation of diffuse and *not* discrete compaction bands might have also been facilitated by the inability of the fragments to break further in the relevant simulations.

#### 4.2. The effect of the bond strength

The effect of the bond strength was investigated in simulations where 8 fragments were introduced to the simulation after a grain breakage event. Fig. 8 contains plots of the stress-strain curves for three simulations performed on the same sample with precisely the same shortening rate, bond locations and boundary conditions, but with varying bond strengths. As one can observe, lowering the bond strength made the sample more stable, increasing its ductility. As already discussed, for large bond strength a large brittle peak was observed, associated with a sudden stress-drop and a large negative sample stiffness. As the bond strength was

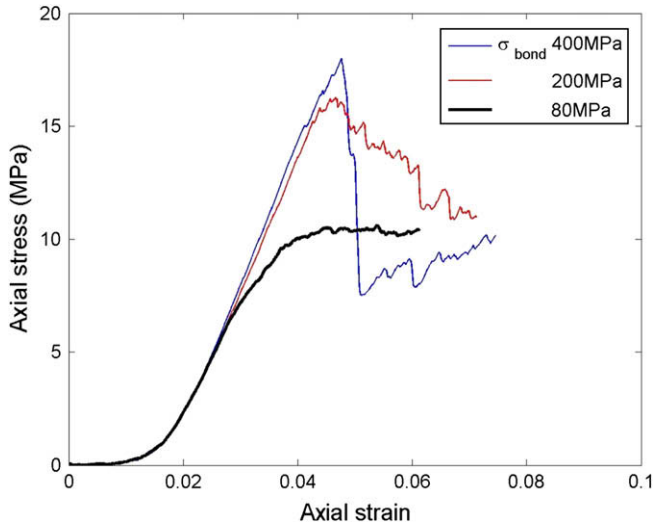


**Fig. 8.** The stress versus strain for simulations where 8 fragments replaced each broken grain and the cementation bond strength was varied.

decreased the stress-drop became less abrupt and the maximum stress attained by the sample (the sample strength) decreased.

The difference in the behaviour was a consequence of the number of bonds broken prior to the crushing peak. For a very similar simulation with a high bond strength (400 MPa – see Fig. 4), the structure of the sandstone remained intact with very few bonds broken before the crushing peak. As the bond strength decreased, the number of bonds broken before significant particle crushing increased, progressively turning the sandstone to a sand. One might nevertheless be puzzled as to why the sandstone had an increased strength when compared to a less bonded material resembling sand, especially as the samples tested in the simulations of Fig. 8 were initially the same.

In order to investigate whether the presence of bonds affected the inter-particle force distribution, so causing this difference in sample strength, the force distribution inside a sand and a sandstone sample were compared. Fig. 9a plots the probability density function (pdf) for the maximum normal contact force on each grain (maximal force) in sandstone as non-dimensionalised by its mean value for three different stress levels. The plot also includes the mean pdf for the same sample with completely unbonded and unbreakable grains (a sand – more extensively reported in

Marketos and Bolton, 2007). These data were derived from simulations where bond and grain breakage were completely suppressed. In addition, the forces in a region extending 9 mm from the top and bottom boundaries were not sampled so as to avoid boundary effects.

One observes that the curves for sand and sandstone were very similar. The main difference lay in forces smaller than the mean which do not affect grain crushing. A very small difference could also be observed for large force magnitudes, with the sandstone showing a small and insignificant bias towards larger forces. However, this would make the observation of a higher sample strength for sandstone even more counter-intuitive.

In an attempt to explain the higher sample strengths for sandstone, the dependence of the force on the particle radius was examined. Fig. 9b plots the mean maximal particle force in a specific grain size range versus grain radius for sandstone. The average non-dimensionalised maximal force on grains with a specific radius was found to be independent of stress level and to increase linearly with grain size. A very similar linear relationship was also documented for sand (see Marketos and Bolton, 2007). As implied by Eq. (1) the crushing criterion implemented here dictated that the force needed to crush a particle was proportional to its radius squared. However, on average a grain attracted a force proportional to its radius. This had the initial effect of preferentially crushing the smallest particles, both in sand and sandstone.

The main difference between sandstone and sand was that in the former the strong-force network was fixed in space by means of the bonds. In sandstone the force carried by the crushed particle was redistributed in the immobile force-carrying grain network. The probability of this extra force falling on a weak sandstone particle (i.e. the probability of a further crush) was therefore small, as it would correspond to the probability of finding two weak particles on the strong-force network relatively close to each other. This was exacerbated by the fact that strong forces preferentially passed through large and therefore stronger particles.

On the other hand the grains in sand were freer to move locally, constantly altering the position of the local strong-force network. It therefore became more probable, after an initial crushing event that a strong-force chain would fall on another weak particle, breaking it. The effect of this was that more crushing was observed in the sand at lower stress levels, with the fully bonded sandstone sample remaining stable until larger stresses. The difference in the probability of crushing was further illustrated by the stress at which the first event occurred. This was 6.9 MPa for sand but 8.0 MPa for sandstone (see Figs. 4 and 10 respectively).

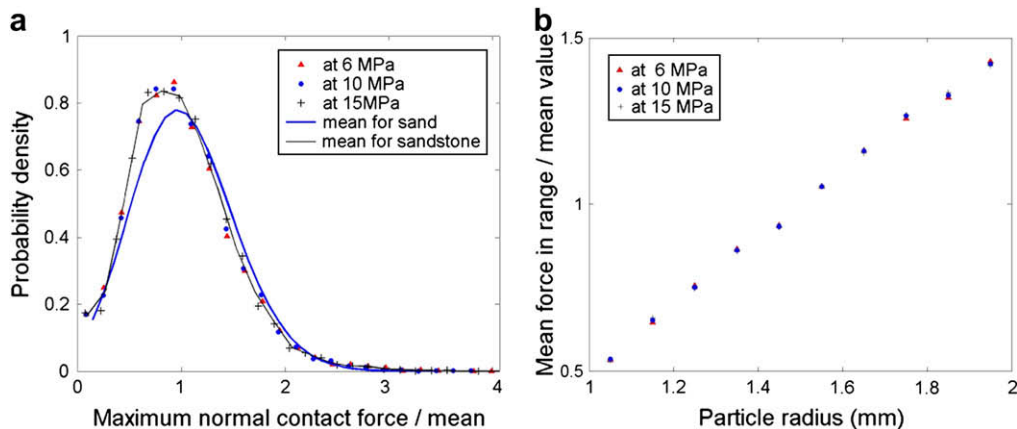


**Fig. 9.** (a) The probability density function of maximal normal contact force over mean maximal contact force for three different stress levels of sandstone compared to the mean curve for sand. (b) The mean of the maximal normal contact force in each particle size range (as non-dimensionalised by the mean value for all particles) versus particle radius for three different stress levels in sandstone.

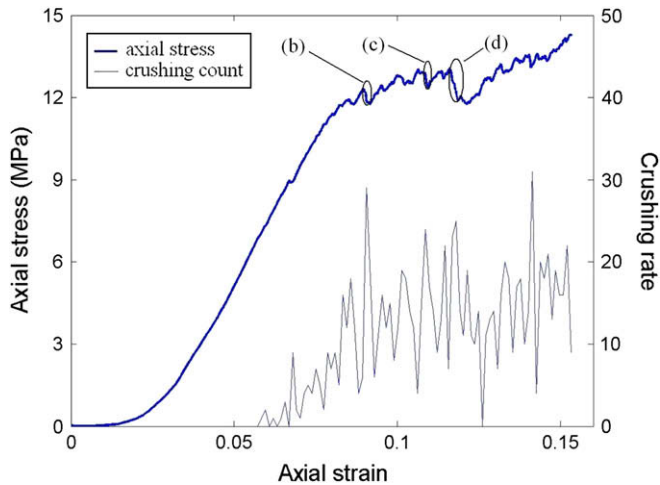


**Fig. 10.** The vertical stress and crushing rate (similar to acoustic emission data) versus strain for the simulated sand when crushing is suppressed inside a 9 mm wide region at the top and bottom boundaries.

## 5. Grain crushing in sand

A set of one-dimensional compression simulations was performed on the sample with the grains unbonded so as to test whether compaction bands would equally develop in sand. Particle crushing was represented by particle removal for these simulations. Marketos and Bolton (2005) observed that when grain crushing was allowed throughout the sample, well-defined compaction bands localised exactly at the top and bottom boundaries. The simulations that produced this unwanted localisation due to boundary effects will not be presented here.

When grain crushing was suppressed in a region extending 9 mm (3 grain diameters) from the top and bottom ends of the sample (see Section 3.3), this unwanted localisation was also

suppressed. The stress–strain and crushing count curves for such a one-dimensional compression test are shown in Fig. 10. A history of crushing events similar to acoustic emission data reported in experiments is also included. As one observes in Fig. 10, crushing of particles was initiated at a strain of approximately 0.06. It reached a constant mean level of about 10 events per 0.0008 strain interval, and shortening was dominated by particle crushing after a strain of roughly 0.09.

The stress–strain curve exhibited instabilities. Its peaks and drops were associated with peaks and drops in the number of crushing events observed. Fig. 11 plots the locations of the crushing events corresponding with these drops (i.e. points marked (b), (c) and (d) on Fig. 10). Here one can observe that during the stress-drop crushing was fairly localised and remote from the top and bottom boundaries. Crushing localisation was not so pronounced as in sandstone, but the results here indicated that it might occur in an unbonded granular material also. A plot of all the particle crushing events is included in Fig. 11a. One can see here that crushing was not localised as a whole, although more crushing was observed towards the bottom of the specimen, corresponding to the location of this mild compaction localisation. Crushing events occurring outside this region were found to correspond to instants of strain-hardening after a stress-drop.

## 6. Instability and compaction bands

### 6.1. Crushing events up to the stress peak

The discussion will now focus on the sequence of events leading to the observed sample instability for the sandstone with the strongest bonds (bond strength of 400 MPa), where 8 particle fragments were introduced to model grain breakage. The stress–strain curve for this simulation is plotted again in Fig. 12a with points A–E marked on it, between which the locations of crushing events inside the sample will be shown.

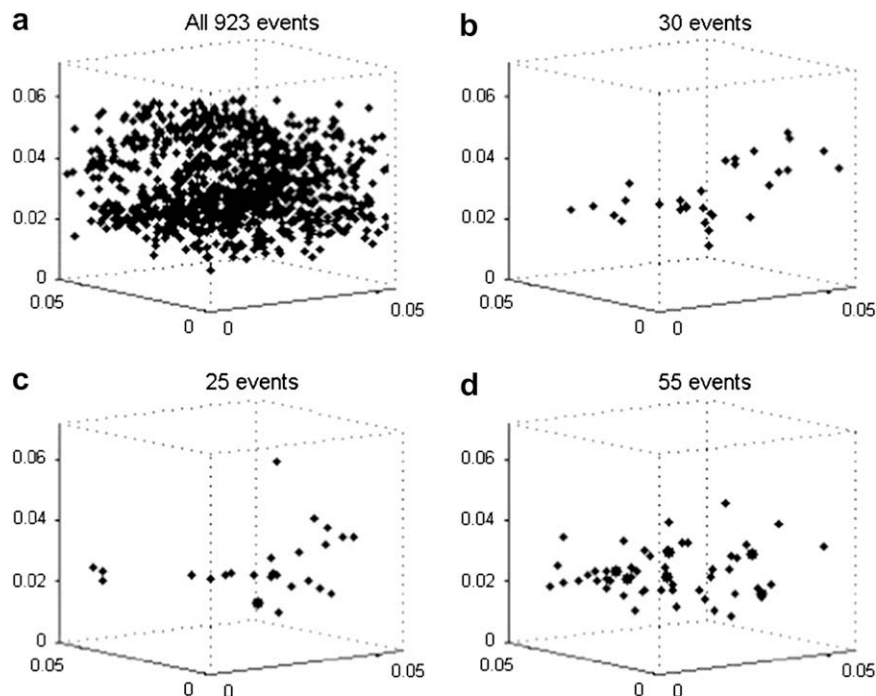


**Fig. 11.** A plot of the location of crushing events inside the cubical element for a strain increment of (a) the whole simulation and (b), (c), (d) as marked on Fig. 10. These correspond to the simulated sand when crushing is suppressed inside a 9 mm wide region at the top and bottom boundaries. Sample dimensions are in meters.

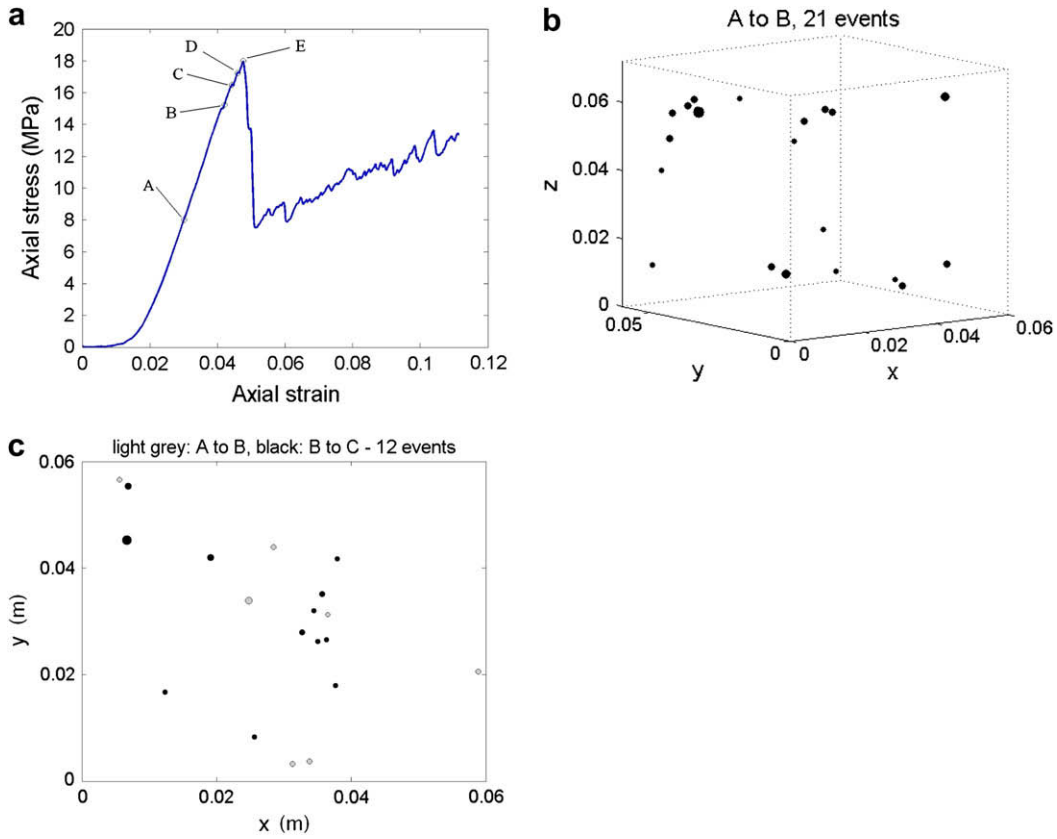


**Fig. 12.** (a) The axial stress versus axial strain for the sandstone simulation with a bond strength of 400 MPa and where crushing is modelled by replacement of the parent particle by 8 fragments. (b) A three-dimensional plot of the crushing locations between points A and B. (c) The projection on the  $x$ - $y$  plane of the crushing locations for the strain increments of A–B (light grey) and B–C (black). Sample dimensions are in meters.

The first crushing event occurred at point A, at a stress of 8 MPa and a strain of 0.03. Fig. 12b plots the events between points A and B in three-dimensional space. One observes that the location of the 21 initial crushing events was fairly random, although most crushing occurred towards the top and bottom ends of the sample. The events from A to B can be said to define the initial phase of crushing, with individual crushes not affecting each other (i.e. being statistically independent).

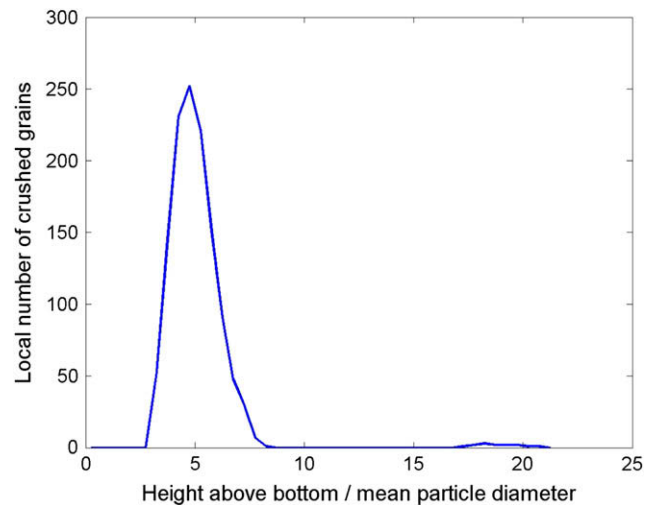
After point B the majority of crushing events (more than 99%) concentrated on a band parallel to the  $x$ - $y$  plane and approximately 5 mean diameters wide (see Fig. 13), the centres of crushed particles lying at heights between 9 and 23 mm above the bottom platen. This is similar to the band width of 3–4 grain diameters observed by Louis et al. (2006) in the laboratory. In subsequent plots events lying outside the main compaction band region were neglected as irrelevant to the crushing localisation. Also, only the projection of the location of crushing events on the  $x$ - $y$  plane will be shown, as the events all roughly occurred on the plane of the compaction band.

Fig. 12c plots the location of the crushing events between A and B on the  $x$ - $y$  plane in light grey. Of the 21 events only 7 were plotted, as the rest lay out of the compaction band region. These events were fairly evenly scattered on the plane. The events between B and C, however, all occurred inside the compaction band region and a nucleation of events around point (0.035, 0.03) was observed. During this stage of deformation crushing was stable and events occurred at increasing sample stress.

Fig. 14b plots the locations of crushing events between C, C1 and D. The events between C and C1 concentrated around a previous crushing event, i.e. around a local stress concentration at the point

(0.025, 0.010). During this strain increment crushing propagated in an unstable fashion, as demonstrated by the macroscopic stress-drop observed during the event. However, the propagation of the crushing localisation was arrested, as the surrounding material was finally able to carry the additional stress. Events from C1 to D occurred at a different location while the sample stress increased.

Fig. 15b plots the locations of crushing events between D and E. During this stage of deformation the sample stress increased in



**Fig. 13.** A plot of the local number of crushed particles versus distance from the bottom end of the band as non-dimensionalised by the mean particle diameter.

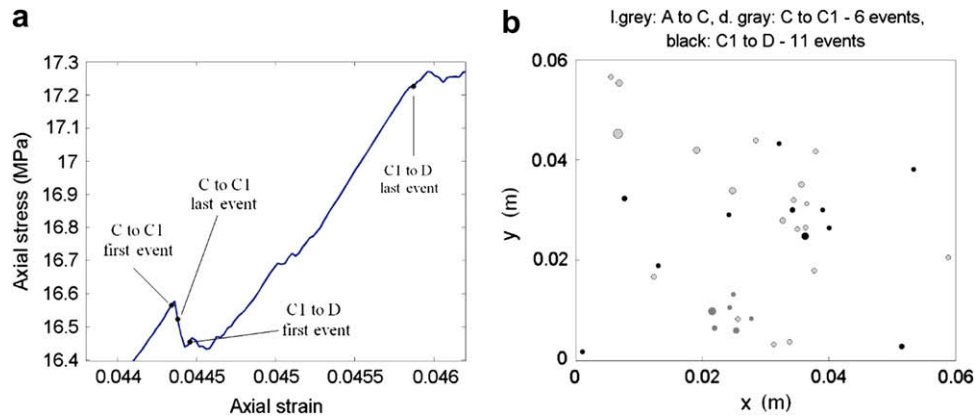


**Fig. 14.** (a) A detailed version of the stress–strain plot of Fig. 12a showing points C, C1 and D. (b) The projection on the  $x$ – $y$  plane of the crushing locations for the strain increments of A–C (light grey) C–C1 (darker grey) and C1–D (black).

a stable fashion. However, crushing again concentrated around a point, which this time was (0.04, 0.03). The pre-peak behaviour of the sample can therefore be summarised as consisting of the following stages. First random grain breakage occurred, eliminating weak particles that happened to be on the strong-force network. Then crushing events started interacting with each other, as stress-concentrations developed. Two regions of fairly local crushing could be observed, the formation of one of which was associated with an instability that did not fully propagate. The other crushing localisation continued growing in a more stable fashion until by point E it had reached a critical size. This point marked the beginning of the unstable collapse of the sample, associated with propagation of the crushing localisation inside a band.

### 6.2. The propagation of the compaction band

The plots of Fig. 15 show the incremental propagation of the compaction band 20 events at a time (with the exception of Fig. 15h, where approximately 100 events are shown). Fig. 15a shows the relevant points (E–Q) on the stress–strain curve. One can observe that the crushing events spread out from the initiation point. At each point the crushed region could be envisaged as a circle (or an ellipse). The crushed region did not grow by expanding its radius, i.e. by adding new crushed particles around its whole perimeter. At each stage, rather, only a section of the boundary of the compaction band could be considered active, with new crushing events occurring there.

## 7. Predicting the stress at which the instability propagates

A simplified calculation will be presented here in an attempt to predict the stress at which the stress-drop occurs and crushing propagates through the sample in an unstable fashion. The method is based on calculating probabilities for individual grain crushing events on the basis of the contact force on a grain exceeding its maximum attainable value (grain strength – see Eq. (1), similar to Marketos and Bolton, 2007). However this time a calculation of the probability of local force redistribution caused by a crushing event around broken grains is also needed, so as to calculate the probability of further crushing events occurring after such a first event, and so approach propagation. A series of approximations have been included in the calculation, but it should in principle be possible to perform the same procedure in a more rigorous manner.

The first particles to crush in the simulations were the weakest ones ( $F_{\text{strength}}$  160–200 N when  $\sigma_{\text{crush}}$  is 40 MPa and the grain

radius is 1 mm) which happened to be on a strong-force chain. Therefore the condition for the first few crushes, when crushing locations were still independent of each other, can be written as  $3 F_{\text{mean}} > 200$  N, as Fig. 9a implies that there are not many particles with forces larger than  $3 F_{\text{mean}}$ . This leads to an  $F_{\text{mean}}$  of approximately 70 N. In the sandstone with the strong cementation bonds the particles were relatively immobile and the strong-force network relatively fixed. The crushed particles therefore left a void in the strong-force network as the fragments could not carry any force and the force previously carried by them was locally redistributed to neighbouring particles. If one assumes that the force on a crushed grain would be entirely redistributed to 3–4 neighbouring particles then each would carry an additional force of 0.75–1 times  $F_{\text{mean}}$ . As the sample was stressed one might further assume that the force network remained immobile and that the particles around the first crush continued to carry the extra force of 0.75–1 times  $F_{\text{mean}}$ . If this extra force again fell on a weak particle ( $F_{\text{strength}} < 200$  N) it would crush it, creating an even greater force concentration in the region around the crushed particles. One should think of this phenomenon as analogous to a cavity or flaw inside an elastic plate creating a local stress concentration.

At some point the force concentration around the broken particles would become so large that even the stronger particles would break. With additional particle breakage the force concentration would increase further and breakage would propagate in an unstable fashion. For the simulations presented here one might identify the condition for the instability as enough weak particles ( $F_{\text{strength}} < 200$  N) breaking at a specific region. Each of these broken particles would be carrying a force of 0.75–1 times  $F_{\text{mean}}$ , leading to an approximate prediction of localisation as occurring at an  $F_{\text{mean}}$  of between 200 and 270 N for the whole sample.

An approximate relation between  $F_{\text{mean}}$  and vertical stress will now be sought. Particles (9000) were contained in a volume of  $7.2 \times 6 \times 6$  cm leading to the conclusion that  $(9000/1.2)^{2/3}$ , i.e. approximately 400 particles corresponded to the platen area of  $6 \times 6$  cm. Assuming that the force was evenly distributed within each layer of 400 particles, the mean force  $F_{\text{mean}}$  can be calculated as  $\sigma \times 0.06^2/400 = 9 \times 10^{-6}\sigma$ . Therefore the stress corresponding to a mean force of 200–270 N and the onset of the crushing localisation can be calculated as 22–30 MPa. This approximate result is of the same order of magnitude as that observed in the simulations (18 MPa), even though the method for its estimation involved some rather crude assumptions, highlighting the potential of such a micromechanics based method.

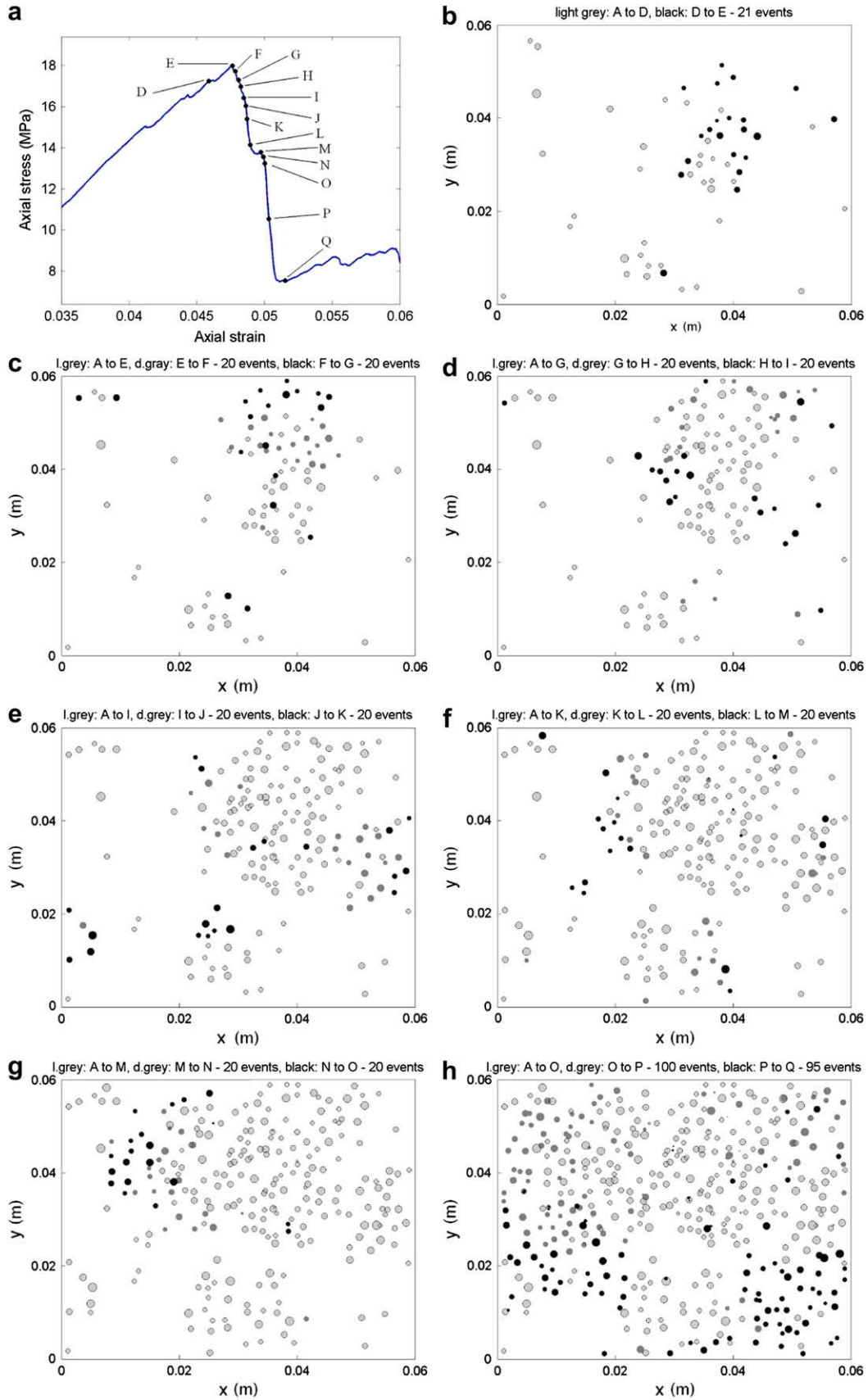


Fig. 15. (a) A stress–strain plot marking points D–Q. (b)–(h) Plots of the incremental propagation of the compaction band as projected on the x–y plane.

## 8. Concluding remarks

Both discrete and diffuse compaction bands were reproduced in the simulations. The most pronounced discrete compaction bands were observed in the simulations on sandstone with a high cementation bond strength (see Figs. 4, 8 and 15). The stress for compaction band propagation was related to the crushing strength of the weakest particles, as confirmed by a simplified calculation outlined in Section 7. The authors believe that a similar micromechanical approach, based on calculating probabilities for individual crushing events, holds the key to linking grain-scale (e.g. grain strength) and continuum mechanics parameters (e.g. the stress at which a band propagates).

Data presented here also allowed for the identification of grain-scale properties (cementation bond strength, grain fragmentation mode) that are linked to compaction band formation but which had eluded previous investigations. The value of the bond strength in relation to the grain strength is clearly important as it controls the number of bonds broken before significant grain breakage occurs. A high bond strength leads to a marked instability and a clear compaction band. In the simulations, lowering the bond strength increased the ductility of the sample and made localisation less marked.

In addition the peak stress attained by the sample was decreased. The observed decrease of the sample strength might be attributed to the simple grain breakage criterion used. Different breakage criteria or grain strength distributions might eliminate this effect, and this point needs to be further investigated. However, what seems clear is that compaction bands form more easily in sandstone than in sand with the same grain properties due to the immobility of grains in the former. Simulations on sand have produced instabilities that were linked to crushing localisation of a limited extent. This has indicated that compaction band formation is possible in sand also, even though the formation of well pronounced discrete bands possibly also requires special conditions on grain uniformity.

Another important conclusion from the current study is that the post-breakage grain behaviour affects compaction band formation. This is significant as the grain fragmentation mode is related to grain mineralogy and the extent of internal flaws and microfractures in a grain. Little difference was observed between simulations where grain crushing was modelled by particle removal and simulations where the broken particle was replaced by 8 fragments. This was because the grain fragments fell into the inter-grain space and so were unable to carry force in the strain increments required for compaction banding.

However, when particle breakage was modelled by a reduction of the contact stiffness by a factor of 2, a diffuse compaction band (as observed by Olsson and Holcomb, 2000) and a less unstable sample behaviour were observed. This therefore indicated that the key grain property leading to diffuse compaction banding is the post-breakage behaviour of the grains and more specifically their ability to carry a significant amount of force after they are broken. It remains unclear, however, whether an advancing crushing front can be observed in the field, where the boundary and loading conditions are very different.

## Acknowledgements

The first author would like to thank the A.S. Onassis and A.G. Leventis Foundations for their invaluable financial assistance.

## References

Baud, P., Klein, E., Wong, T.-F., 2004. Compaction localization in porous sandstones: spatial evolution of damage and acoustic emission activity. *Journal of Structural Geology* 26 (No. 4), 603–624.

- Cheng, Y.P., Nakata, Y., Bolton, M.D., 2003. Discrete element simulation of crushable soil. *Géotechnique* 53 (No. 7), 633–641.
- Couroyer, C., Ning, Z., Ghadiri, M., 2000. Distinct element analysis of bulk crushing: effect of particle properties and loading rate. *Powder Technology* 109, 241–254.
- Cundall, P.A., Strack, O.D.L., 1979. A discrete numerical model for granular assemblies. *Géotechnique* 29 (No. 1), 47–65.
- DiGiovanni, A.A., Fredrich, J.T., Holcomb, D.J., Olsson, W.A., 2001. Microscale damage evolution in compacting sandstone. In: Couples, G., Meredith, P., Main, I. (Eds.), *Fracture, Damage and Related Deformation Features*. Geological Society of London, Special Publication.
- Haimson, B.C., 2001. Fracture-like borehole breakouts in high-porosity sandstone: are they caused by compaction bands? *Physics and Chemistry of the Earth, Part A: Solid Earth and Geodesy* 26 (No. 1–2), 15–20.
- Hardin, B.O., 1989. Effect of rigid boundaries on measurement of particle concentration. *Geotechnical Testing Journal* 12 (No. 2), 143–149.
- Holcomb, D., Rudnicki, J.W., Issen, K.A., Sternlof, K., 2007. Compaction localization in the Earth and the laboratory: state of the research and research directions. *Acta Geotechnica* 2 (No. 1), 1–15.
- Hyde, A.F.L., Nakata, Y., 1999. Yield and soil crushability. In: *Proceedings of the International Workshop on Soil Crushability, IWSC '99, Ube, Japan*, pp. 1–18.
- Issen, K.A., 2002. The influence of constitutive models on localization conditions for porous rock. *Engineering Fracture Mechanics* 69 (No. 17), 1891–1906.
- Itasca Consulting Group Inc., 2003. PFC<sup>3D</sup>: Particle Flow Code in 3 Dimensions, Version 3.0. Itasca Consulting Group Inc., Minneapolis, USA.
- Katsman, R., Aharonov, E., 2006. A study of compaction bands originating from cracks, notches and compacted defects. *Journal of Structural Geology* 28, 508–518.
- Lobo-Guerrero, S., Vallejo, L.E., 2005. Crushing a weak granular material: experimental numerical analyses. *Géotechnique* 55 (No. 3), 245–249.
- Louis, L., Wong, T.-F., Baud, P., Tembe, S., 2006. Imaging strain localization by X-ray computed tomography: discrete compaction bands in Diemelstadt sandstone. *Journal of Structural Geology* 28 (No. 5), 762–775.
- Marketos, G., 2007. An Investigation of Crushing and Compaction Bands in Granular Material. Ph.D. thesis, Cambridge University, U.K.
- Marketos, G., Bolton, M.D., 2005. Compaction bands as observed in DEM simulations. In: Garcia-Rojo, R., Herrmann, H.J., McNamara, S. (Eds.), *Powders and Grains 2005: Proceedings of the Fifth International Conference on Micro-mechanics of Granular Media*, vol. 2. A.A. Balkema, Rotterdam, Stuttgart, Germany, pp. 1405–1409.
- Marketos, G., Bolton, M.D., 2007. Quantifying the extent of crushing in granular materials: a probability-based predictive method. *Journal of the Mechanics and Physics of Solids* 55 (No. 10), 2142–2156.
- Marketos, G., Bolton, M.D. *International Journal for Numerical and Analytical Methods in Geomechanics*, in press.
- McDowell, G.R., Amon, A., 2000. The application of Weibull statistics to the fracture of soil particles. *Soils and Foundations* 40 (No. 5), 133–141.
- Mollema, P.N., Antonellini, M.A., 1996. Compaction bands: a structural analog for anti-mode I cracks in Aeolian sandstone. *Tectonophysics* 267, 209–228.
- Nakata, Y., Hyde, A.F.L., Hyodo, M., Murata, H., 1999. A probabilistic approach to sand particle crushing in the triaxial test. *Géotechnique* 49 (No. 5), 567–583.
- Nakata, Y., Kato, Y., Hyodo, M., Hyde, A.F.L., Murata, H., 2001. One-dimensional compression behaviour of uniformly graded sand related to single particle crushing strength. *Soils and Foundations* 41 (No. 2), 39–51.
- Olsson, W.A., 2001. Quasistatic propagation of compaction fronts in porous rock. *Mechanics of Materials* 33, 659–668.
- Olsson, W.A., Holcomb, D.J., 2000. Compaction localisation in porous rock. *Geophysical Research Letters* 27 (No. 1), 3537–3540.
- Olsson, W.A., Holcomb, D.J., Rudnicki, J.W., 2002. Compaction localization in porous sandstone: implications for reservoir mechanics. *Oil and Gas Science and Technology-Revue de l'IFP* 57 (No. 5), 591–599.
- Rudnicki, J.W., 2007. Models for compaction band propagation. In: David, C., Le Ravalec-Dupin, M. (Eds.), *Geomechanics and Rock Physics for Reservoir and Repository Characterization: Proceedings of Euroconference on Rock Physics 2005*. Geological Society of London, Special Publication, vol. 284, pp. 107–125, doi:10.1144/SP284.8.
- Rudnicki, J.W., Sternlof, K.R., 2005. Energy release model of compaction band propagation. *Geophysical Research Letters* 32, L16303.
- Sternlof, K.R., Rudnicki, J.W., Pollard, D.D., 2005. Anticrack-inclusion model for compaction bands in sandstone. *Journal of Geophysical Research* 110, B11403.
- Sternlof, K.R., Karimi-Fard, M., Pollard, D.D., Durloufsky, L.J., 2006. Flow and transport effects of compaction bands in sandstone at scales relevant to aquifer and reservoir management. *Water Resources Research* 42 (7), W07425.
- Takei, M., Kusakabe, O., Hayashi, T., 2001. Time-dependent behavior of crushable materials in one-dimensional compression tests. *Soils and Foundations* 41 (No. 1), 97–121.
- Tembe, S., Baud, P., Wong, T.-F., 2008. Stress conditions for the propagation of discrete compaction bands in porous sandstone. *Journal of Geophysical Research* 113, B09409, doi:10.1029/2007JB005439.
- Tsoungui, O., Vallet, D., Charmet, J.-C., 1999. Numerical model of crushing of grains inside two-dimensional granular materials. *Powder Technology* 105, 190–198.
- Vajdova, V., Baud, P., Wong, T.-F., 2004. Permeability evolution during localized deformation in Bentheim sandstone. *Journal of Geophysical Research* 109, B10406.
- Wang, B., Chen, Y., Wong, T.-F., 2008. A discrete element model for the development of compaction localization in granular rock. *Journal of Geophysical Research* 113, B03202.